

The Shape of Copper Oxide Clusters Under Oxygen Excess

A Genetic Algorithm Search

Master's thesis in Applied Physics

Oskar Larsson

MASTER'S THESIS 2017

The Shape of Copper Oxide Clusters Under Oxygen Excess

A Genetic Algorithm Search

Oskar Larsson



CHALMERS
UNIVERSITY OF TECHNOLOGY

Department of Physics
Division of Chemical Physics
CHALMERS UNIVERSITY OF TECHNOLOGY
Gothenburg, Sweden 2017

The Shape of Copper Oxide Clusters Under Oxygen Excess
A Genetic Algorithm Search
Oskar Larsson

© OSKAR LARSSON, 2017.

Supervisor and Examiner: Anders Hellman, Department of Physics

Master's Thesis 2017
Department of Physics
Division of Chemical Physics
Chalmers University of Technology
SE-412 96 Gothenburg
Telephone +46 31 772 1000

Cover illustration

Top right: Free energy diagram for $[\text{Cu}_6\text{O}_{3-9}]^+$ (top) and $[\text{Cu}_6\text{O}_{3-9}]^-$ (bottom). See Figure 4.3 for further information.

Bottom: Statistics for genetic algorithm simulations of $[\text{Cu}_6\text{O}_6]^-$. Further explained in Figure 4.1.

In front: Example of genetic algorithm step (pairing). The step shows the global minimum structure of $[\text{Cu}_6\text{O}_6]^-$ being found.

Typeset in L^AT_EX
Printed by Chalmers Reproservice
Gothenburg, Sweden 2017

The Shape of Copper Oxide Clusters Under Oxygen Excess
A Genetic Algorithm Search
Oskar Larsson
Department of Physics
Chalmers University of Technology

Abstract

The stability of copper oxide clusters was investigated using density functional theory (DFT) where the exchange-correlation was described by the Perdew-Burke-Ernzerhof generalized gradient approximation. In particular, the $\text{Cu}_{1-3}\text{O}_{1-6}$ and $[\text{Cu}_6\text{O}_{3-9}]^{+/-}$ clusters were investigated. To estimate the stability, the free energy of the oxidized cluster was compared to the free energies of the corresponding bare cluster and gas phase molecular oxygen. A genetic algorithm was used to find the lowest energy shapes of the clusters.

For the neutral clusters, the structures found by the genetic algorithm were compared to structures found in previous theoretical studies. In many cases the results agreed. In those cases they did not, the cause of the difference was ascribed to the different exchange-correlation functionals that were used in the DFT calculations. Regarding the stability, many of the oxygen-rich clusters had a low free energy at room temperature.

The results for the charged clusters were compared to experiments measuring the relative abundance of copper oxide clusters of different compositions. The trends found in this thesis are similar to those found experimentally. For example, at room temperature, experiments found $[\text{Cu}_6\text{O}_7]^+$ to be the most abundant composition for the cations. This is in good agreement with the results found in this thesis. Similarly for the anions, theoretical and experimental results agree on $[\text{Cu}_6\text{O}_5]^-$ being the most stable composition.

Keywords: copper oxide clusters, DFT, density functional theory, PBE, genetic algorithm, free energy

Acknowledgements

First and foremost I would like to thank my supervisor Anders Hellman for coming up with, and guiding me through the project. I would also like to thank everyone at the division of Chemical Physics, for always answering questions, discussing physics and creating an excellent work environment. Additionally, I am grateful for all support and encouragement from my friends and family.

All calculations were performed at the computer center C³SE at Chalmers, with CPU time provided through a SNIC grant.

Oskar Larsson, Gothenburg, April 2017

Contents

List of Figures	xi
List of Tables	xiii
1 Introduction	1
1.1 Summary	1
1.2 Preceding Experimental Results	2
2 Density Functional Theory	3
2.1 Schrödinger Equation	3
2.2 Electron Density	4
2.3 Kohn-Sham Equations	4
2.4 Implementation	6
2.5 Approximations	7
2.6 Free Energy	8
2.7 Computational Method	10
3 Optimization	13
3.1 Local Structure Optimization	13
3.2 Global Structure Optimization	14
3.2.1 Genetic Algorithms	14
3.2.2 Local Implementation	15
4 Results	19
4.1 Local Structure Optimization	19
4.1.1 Molecular Adsorption	19
4.1.2 Bulk Stoichiometry	20
4.2 Global Structure Optimization	21
4.2.1 Statistics $[\text{Cu}_6\text{O}_{3,6}]^-$	21
4.2.2 Stability of Copper Oxide Clusters	23
4.2.3 Previous Results $\text{Cu}_{1-3}\text{O}_{1-6}$	26
5 Conclusion	29
5.1 Genetic Algorithm	29
5.2 Copper Oxide Clusters	30
Bibliography	31

A	Appendix	35
A.1	Local Minima	35
A.2	Global Minima	36
A.3	Comparing Top Candidates	38

List of Figures

1.1	Experimental results for copper oxide clusters	2
4.1	GA statistics	22
4.2	Stability of $\text{Cu}_{1-3}\text{O}_{1-6}$	24
4.3	Stability of $[\text{Cu}_6\text{O}_{3-9}]^{+/-}$	25
A.1	Top candidates GA	38

List of Tables

2.1	Basis sets for O and Cu	11
2.2	Comparing spin-polarized and non spin-polarized calculations	11
3.1	Settings local optimization	14
4.1	Molecular oxygen adsorption	20
4.2	Enthalpy of formation for $(\text{Cu}_2\text{O})_n$	21
4.3	Charged Cu_2 and Cu_2O	21
4.4	GA statistics	23
4.5	Previous results $\text{Cu}_{1-3}\text{O}_{1-6}$	26
4.6	Different ground state structures $\text{Cu}_{1-3}\text{O}_{1-6}$	27
A.1	Local minima bare clusters	35
A.2	Global minima $\text{Cu}_{1-3}\text{O}_{1-6}$	36
A.3	Global minima $\text{Cu}_6^{+/-}$	37
A.4	Global minima $[\text{Cu}_6\text{O}_{3-9}]^{+/-}$	37

1

Introduction

In this thesis the stability of copper oxide clusters was studied. Copper oxide clusters play an important role in many catalytic reactions, such as, NO_x reduction^[1] and methane-to-methanol conversion^[2]. In the bulk case, two stable compositions of copper oxide exists: cuprous oxide (Cu₂O) and cupric oxide (CuO). However, the stable compositions for clusters might be different.

1.1 Summary

Two different types of clusters were investigated. The first was neutral clusters composed of one to three copper atoms and one to six oxygen atoms. The second was singly charged clusters composed of six copper atoms and three to nine oxygen atoms. In order to estimate the stability of a cluster, density functional theory (DFT) was used. From DFT it was possible to calculate the ground state electronic energy of an atomic system. Chapter 2 explains the theory behind this. The chapter also covers how DFT results can be extended to compute free energies. The stability of a copper oxide cluster was estimated by comparing its free energy to the free energies of the corresponding bare copper cluster and gas phase molecular oxygen. Hence, the more a system can lower its free energy by forming an oxidized cluster from a pure copper cluster and oxygen molecules, the more stable it will be considered to be.

From DFT it is also possible to calculate forces acting on the nuclei of a system. Section 3.1 shows how these forces can be used to perform a local structure optimization of the system. However, to make a fair comparison between the different compositions the most stable structures, i.e. the global minima, should be used. Due to the large amount of possible structures for a cluster, a genetic algorithm (GA) was used to find these. What a GA is and how it was implemented in this thesis is covered in Section 3.2.

In Chapter 4 the results of the calculations are presented and compared to earlier theoretical and experimental work. In most cases the results are in good agreement with previous studies. The GA is also found to perform well for the clusters used in this thesis. Conclusions drawn from the results are presented in greater detail in Chapter 5.

The purpose of the thesis is to:

- Investigate the performance of a GA for the task of finding the most stable structures of copper oxide clusters.
- Find the most stable structures for $\text{Cu}_{1-3}\text{O}_{1-6}$ and $[\text{Cu}_6\text{O}_{3-9}]^{+/-}$.
- In the case of $[\text{Cu}_6\text{O}_{3-9}]^{+/-}$, investigate how the theoretical relative stabilities of the different compositions compares to experiments.

1.2 Preceding Experimental Results

The relative abundance of copper oxide clusters has been investigated experimentally at the University of Tokyo, by Morita et al. in 2013^[3] and by Mafuné et al. in 2015^[4]. It was found that the number ratios of thermally stable copper oxide clusters lie in between the ratios of the two stable bulk copper oxides CuO and Cu_2O , see Figure 1.1. In the experiment copper clusters were prepared through laser ablation

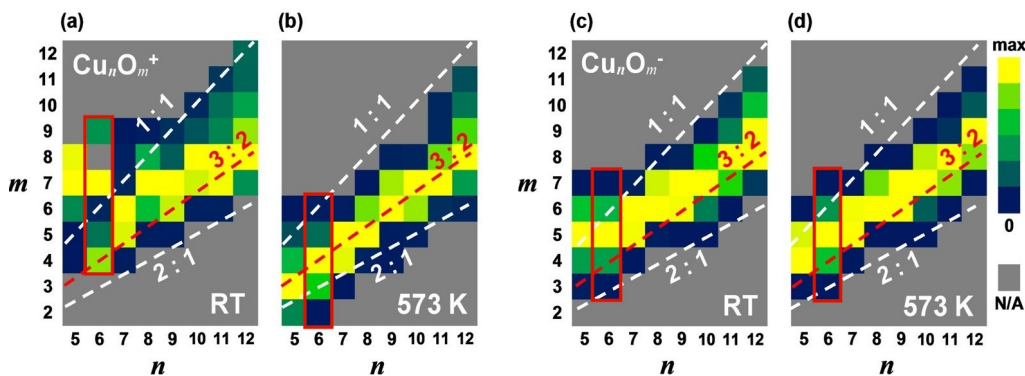


Figure 1.1: Experimental results for the relative abundances of Cu_nO_m^+ and Cu_nO_m^- , normalized in each column of n . In this thesis clusters with $n = 6$ (surrounded by red boxes) are further investigated. Adapted with permission from Morita et al.^[3]. Copyright 2013 American Chemical Society.

of a copper rod which was exposed to oxygen diluted in helium. Mass spectrometry was used in order to determine the relative abundances of different compositions. The experiment was also performed at 623 K; the result was the same as for 573 K.

In the article by Mafuné et al.^[4] it is stated that the distribution of clusters, only considering the number of copper atoms they contain (n), did not change significantly during the experiment. Therefore, by normalizing the data in Figure 1.1 per column the results does not depend on the initial distribution created through the laser ablation. This also simplifies the analysis of the thermal stability as the different n -values can be investigated independently. In the article it is also stated that the distribution of the clusters at a certain temperature is independent of which temperature the clusters had before, i.e. if they were cooled or heated to the desired temperature. This suggest that it is largely thermodynamical properties rather than kinetic effects that determine the distribution of clusters.

2

Density Functional Theory

Many properties of an atomic system can be determined from its electronic structure. Using DFT, we can calculate the ground state electronic structure. This chapter starts off by briefly explaining how DFT works and why we want to use it. Section 2.6 will go through how we can combine our DFT results with thermodynamics to calculate the free energy of our systems. In the end of the chapter the computational method for the DFT calculations is covered.

2.1 Schrödinger Equation

The mass of the nuclei is much larger than the electron mass. However, the forces acting upon the particles are of the same magnitude. We use this to motivate a separation of the electronic and nuclear time dependence.^[5] This is known as the Born-Oppenheimer approximation^[6]. Freezing the nuclei in space removes the nuclear kinetic energy from the description of our system. It also makes the electronic structure independent of the internuclear potential. We write down the time-independent Schrödinger equation for our system under the Born-Oppenheimer approximation. For a system of N electrons we have:

$$\begin{aligned}\hat{H}\Psi(\mathbf{x}_1, \dots, \mathbf{x}_N) &= E\Psi(\mathbf{x}_1, \dots, \mathbf{x}_N) \\ \text{with } \hat{H} &= \hat{T} + \hat{V}_{\text{ee}} + \hat{V}_{\text{en}}.\end{aligned}\tag{2.1}$$

Here, both the spatial coordinates and the spin coordinate for electron i are represented by \mathbf{x}_i . The kinetic energy operator for the electrons is \hat{T} . The \hat{V} terms are the potential energy operators; \hat{V}_{ee} describes the interaction between electrons and \hat{V}_{en} describes the interaction between electrons and nuclei. In atomic units these operators are:

$$\hat{T}_e = -\frac{1}{2} \sum_i \nabla_i^2, \quad \hat{V}_{\text{ee}} = \frac{1}{2} \sum_{i \neq j} \frac{1}{|\mathbf{r}_i - \mathbf{r}_j|}, \quad \hat{V}_{\text{en}} = -\sum_I \sum_i \frac{Z_I}{|\mathbf{r}_i - \mathbf{R}_I|}$$

where \mathbf{r}_i is the position of electron i , \mathbf{R}_I is the position of nucleus I , ∇_i^2 is the Laplacian for electron i and Z_I is the atomic number of nucleus I . Worth noting is that even though the internuclear repulsion does not affect the electronic structure, its contribution to the energy is still important when comparing different systems.

Even after applying the Born-Oppenheimer approximation, solving our problem numerically quickly becomes unmanageable as the number of electrons increases. To calculate a matrix representation of the Hamiltonian we only have to account for one constant configuration of the nuclei. However, we still need to account for every possible electronic configuration. If we represent space using x grid points, this becomes x^N configurations for N electrons.

2.2 Electron Density

The electron density, $n(\mathbf{r})$, is a probability density for the spatial distribution of electrons. Integrating it over all of space gives the total number of electrons in our system. For a system of N electrons described by the many-body wave function Ψ it is defined as:

$$n(\mathbf{r}) = N \sum_{s_1} \dots \sum_{s_N} \int d\mathbf{r}_2 \dots \int d\mathbf{r}_N |\Psi(\mathbf{r}_1, s_1, \mathbf{r}_2, s_2, \dots, \mathbf{r}_N, s_N)|^2 \quad (2.2)$$

where \mathbf{r}_i are the spatial coordinates of the electrons and s_i are their spin coordinates. In 1964 Hohenberg and Kohn formulated two theorems regarding the electron density of electrons moving in an external potential.^[7] Their first theorem tells us that it is possible to construct a unique energy functional for our system, depending only on the electron density. From the second theorem we know that by minimizing this functional, with regard to the density, we will find the ground state density and energy of our system.

If we use the electron density instead of the many-body wave function to compute the electronic energy, our electronic structure problem might be possible to solve. This is of course highly dependent on the form of the unique functional mentioned in Hohenberg and Kohn's theorems. In the next section we will see how such a functional can be constructed and used to calculate ground state electron densities as well as the corresponding energies.

2.3 Kohn-Sham Equations

To determine the electronic structure of a system we will map the many-body problem described by Equation 2.1 to a single-body problem. This process was first described in 1965 by Kohn and Sham.^[8] We start by replacing the interacting electrons with non-interacting particles, Kohn-Sham electrons, moving in a potential which compensates for the loss of all many-body effects. For such a system it is possible to find the ground state density and energy.

First spin paired systems will be treated. In Section 2.4 we will adapt the theory to work without this restriction. According to the first Hohenberg-Kohn theorem it should be possible to describe any external potential using only the electron density.

In the theory of Kohn and Sham this density is constructed from the lowest lying single particle orbitals, ψ_i , of their independent particles:

$$n(\mathbf{r}) = \sum_{i=1}^N |\psi_i(\mathbf{r})|^2. \quad (2.3)$$

As our system is spin paired, two identical versions of each calculated orbital will exist.

Using single particle orbitals instead of the many-body wave function makes our problem possible to solve numerically. For example, if space is represented using x grid points we only need $N \cdot x$ values to store all the single particle orbitals of N particles compared to the x^N values needed for the many-body wave function.

According to the second Hohenberg-Kohn theorem the ground state density will minimize the energy functional. We write our energy functional as follows:

$$E[n] = T_0[n] + E_H[n] + E_{\text{ext}}[n] + E_{\text{xc}}[n]. \quad (2.4)$$

The first three terms we know how to calculate. These are the kinetic energy for independent particles, the Hartree energy i.e. the Coulomb interaction between electrons, and the energy from the external potential, i.e. Coulomb interaction between the nuclei and the electrons. The two latter are expressed in the following way:

$$E_H[n] = \frac{1}{2} \int d\mathbf{r} d\mathbf{r}' \frac{n(\mathbf{r})n(\mathbf{r}')}{|\mathbf{r} - \mathbf{r}'|} \quad \text{and} \quad E_{\text{ext}}[n] = \int d\mathbf{r} V_{\text{ext}}(\mathbf{r})n(\mathbf{r})$$

where $V_{\text{ext}}(\mathbf{r})$ is the potential from the nuclei.

Looking at the expression for E_H , we notice a problem. The electrons are treated as if they interact with themselves. For instance, there is a contribution even for a single electron system. This is referred to as “self-interaction error” and it is unavoidable as we need all our independent particles to feel the same potential. The self-interaction error is counteracted in the exchange term. If exchange is treated exactly, as in Hartree-Fock theory, the error will be canceled out completely. In DFT where exchange is treated approximately, the quality of the cancellation will depend on how good the approximation is.

In contrast to the Hartree and exchange energy, the kinetic energy is not as straight forward to calculate from an electron density. This is the reason we need the single-particle orbitals. By applying the variational method to the energy functional we will find states that have a possibility of minimizing our energy functional for a given density. As our particles are independent, the minimization can be performed independently for each orbital. Adding the constraint that each orbital should have a total probability of one, the variational method becomes:

$$\frac{\delta E}{\delta \psi_i^*} = \epsilon_i \frac{\delta}{\delta \psi_i^*} \left(\int \psi_i^*(\mathbf{r})\psi_i(\mathbf{r}) d\mathbf{r} - 1 \right). \quad (2.5)$$

Here ϵ_i are the Lagrange multipliers from including the constraint. By calculating the functional derivatives, we get the single orbital Kohn-Sham equation:

$$\left[-\frac{1}{2}\nabla^2 + \int d\mathbf{r}' \frac{n(\mathbf{r}')}{|\mathbf{r} - \mathbf{r}'|} + V_{\text{ext}}(\mathbf{r}) + \frac{\delta}{\delta n(\mathbf{r})} E_{\text{xc}}[n] \right] \psi_i(\mathbf{r}) = \epsilon_i \psi_i(\mathbf{r}). \quad (2.6)$$

This is an eigenvalue problem; its eigenvectors are called Kohn-Sham orbitals. They are the allowed states for a Kohn-Sham electron moving in a potential determined by the given electron density. The eigenvalues can be used to calculate the energy of the system composed of N Kohn-Sham electrons. By multiplying Equation 2.6 with $\psi_i^*(\mathbf{r})$ from the left and summing over the N lowest orbitals we get:

$$\sum_{i=1}^N \epsilon_i = T_0[n] + 2E_H[n] + E_{\text{ext}}[n] + \int d\mathbf{r} n(\mathbf{r}) \frac{\delta}{\delta n(\mathbf{r})} E_{\text{xc}}[n]. \quad (2.7)$$

If we compare this expression with the energy functional we started of with, Equation 2.4, we see that the energy can expressed as:

$$E[n] = \sum_{i=1}^N \epsilon_i - E_H[n] - \int d\mathbf{r} n(\mathbf{r}) \frac{\delta}{\delta n(\mathbf{r})} E_{\text{xc}}[n] + E_{\text{xc}}[n]. \quad (2.8)$$

2.4 Implementation

The lowest lying orbitals of a solution to Equation 2.6 have to reproduce the density used to construct the Hamiltonian. To find such a solution we can start by guessing a density. Using this density we can construct a Hamiltonian and solve the resulting eigenvalue problem. We then use the lowest lying orbitals of this solution to construct a new density which might not match the initial one. Using this new density we can now construct a new Hamiltonian and solve a new eigenvalue problem which will result in yet another density. If these steps are repeated enough times the density will hopefully converge towards its ground state. An overview of the process looks as follows:

1. Guess initial $n(\mathbf{r})$.
2. Use $n(\mathbf{r})$ to construct Hamiltonian and solve resulting eigenvalue problem.
3. Construct new $n(\mathbf{r})$ from solution.
4. Does the new density match the old?
 - Yes \rightarrow solution found!
 - No \rightarrow go to step 2.
5. Calculate energy.

If the highest occupied and lowest unoccupied orbitals are close in energy, there is a risk that the orbital occupation will have significant variations between iterations. This might cause convergence problems. One way of damping these variations is to use smearing, i.e. allowing fractional occupation of the orbitals. The fractional occupation can be determined in different ways. In this thesis a finite-temperature Fermi function is used, ensuring that the correct energy gradients are computed.^[10]

Unrestricted Spin. In reality many systems are not spin paired, e.g. all systems with an odd number of electrons. DFT can be adapted to deal with this problem.

To split spin states, electrons with different spin has to be treated differently somewhere in our calculations. We do this by calculating two separate densities, one for

each spin state. In the energy functional (Equation 2.4), it is only the exchange-correlation term which can have a spin dependence. To get our different spin densities we will simply solve two eigenvalue problems, both very similar to the case of restricted (paired) spin. The only difference is that when calculating the spin up density, the exchange-correlation functional will also depend on the spin-up density and vice versa. The other terms will still only depend on the total density. The exchange-correlation functional for a density only containing one of the spin states could of course differ from the one we use in the spin restricted case. For example, below we see how the exchange functional for a spin paired system can be adapted to the spin unrestricted case.

If the exchange functional for the spin paired system $E_x^{\text{paired}}[n]$ is known, it can be used to express the exchange functional for pure spin densities $n^\uparrow(\mathbf{r})$ or $n^\downarrow(\mathbf{r})$ following way:

$$E_x^{\text{pure}}[n^{\uparrow(\downarrow)}] = \frac{1}{2} E_x^{\text{paired}}[2n^{\uparrow(\downarrow)}]. \quad [11] \quad (2.9)$$

This is possible as a spin paired density is composed of two identical halves, one for each spin state. We can create such a density from a pure spin density by multiplying it by two. To only include the contributions from the original spin state we simply divide the calculated energy by two.

After solving the two eigenvalue problems we can construct our new densities in two different ways. The first is to occupy the orbitals by always choosing the lowest available one without any restriction for the total spin state. This is referred to as converging the spin. If we instead are interested in a specific total spin state, we specify the number of unpaired electrons we want and occupy our orbitals with this restriction in mind. The latter method generally converges faster for a well chosen spin state.

2.5 Approximations

One problem in DFT is that we do not know the exact form of the exchange-correlation energy functional; it has to be approximated in some way. A common assumption in these approximations is that the effects of exchange and correlation are local, i.e. the exchange-correlation contribution at \mathbf{r} , only depends on the electron density at \mathbf{r} . This is called the local density approximation (LDA). For this case we can use expressions for the exchange and correlation energies of a homogeneous electron gas (HEG) to calculate the local contributions.

Exchange should compensate for the fact that electrons in the same spin state can not occupy the same spatial state. The effect of this is that electrons will avoid other electrons with equal spin states. In the case of a HEG with density n_0 the exchange energy per electron is:

$$\epsilon_x(n_0) = -\frac{3}{4} \left(\frac{3}{\pi} n_0 \right)^{\frac{1}{3}}. \quad [9] \quad (2.10)$$

In LDA this leads to the following expression for the exchange energy functional in the spin restricted case:

$$E_x^{(\text{LDA})}[n] = \int d\mathbf{r} n \epsilon_x(n). \quad (2.11)$$

The correlation contributions includes many-body effects originating from the electron Coulomb interaction. An exact analytic form is not known even for the HEG but several parametrized versions exist.^[9]

An improvement of the LDA is the generalized gradient approximation (GGA):

$$E_{xc}^{(\text{GGA})}[n^\uparrow, n^\downarrow] = \int d\mathbf{r} f(n^\uparrow, n^\downarrow, \nabla n^\uparrow, \nabla n^\downarrow).^{[12]} \quad (2.12)$$

Here f is a function which approximates the exchange-correlation energy contribution from a point \mathbf{r} in a semi-local way, using the electron densities for the different spin populations at this point as well as the gradients of the densities at this point. As more information about the system is used more accurate results can be achieved compared to the LDA. The exchange-correlation functional used in this thesis is of this type (see Section 2.7).

2.6 Free Energy

We now know how to determine the electronic structure for a system where the nuclei are fixed in space. However, our goal is to compare theoretical calculations to experimental data. To do this we will calculate the Gibbs free energy (G), i.e. the maximum reversible work that may be performed by our system:

$$G(T, p) = H(T, p) - T \cdot S(T, p). \quad (2.13)$$

Here H is the enthalpy (energy + $p \times$ volume), S is the entropy, T is the temperature and p is the pressure. Under the ideal gas approximation the enthalpy and entropy can be divided in the following way:

$$\begin{aligned} H(T) &= E_{\text{trans}}(T) + E_{\text{rot}}(T) + E_{\text{vib}}(T) + E_{\text{elec}} + k_B \cdot T \\ S(T, p) &= S_{\text{trans}}(T, p) + S_{\text{rot}}(T) + S_{\text{vib}}(T) + S_{\text{elec}}, \end{aligned} \quad (2.14)$$

where k_B is the Boltzmann constant.^[13] The last term in the enthalpy expression is the pressure-volume term rewritten using the ideal gas law and E_{elec} is the ground state electronic energy described in the previous section. Detailed derivations of the other terms are described in Chapter 10 of Cramer 2004^[13]. A quick summary follows.

E_{trans} , E_{rot} . The translational and rotational energies are calculated as $E(T) = \frac{d}{2} k_B T$ where d is the number of degrees of freedom. A cluster has three translational degrees of freedom. If it is linear, it has two rotational degrees of freedom and if it is non-linear it has three.

$S_{\text{trans}}, S_{\text{rot}}$. To calculate the translational entropy we need to know the mass (M) of the cluster. Under the ideal gas approximation this is also the only free energy term which has a pressure dependence. The expression looks like:

$$S_{\text{trans}}(T, p) = k_{\text{B}} \left(\ln \left[\frac{\sqrt{8\pi^3 M^3 k_{\text{B}}^5 T^5}}{ph^3} \right] + \frac{5}{2} \right)$$

where h is Planck's constant.^[13]

To calculate the rotational entropy the clusters are treated as rigid rotors. The resulting expressions in the linear and non-linear case are:

$$S_{\text{rot}}^{\text{linear}}(T) = k_{\text{B}} \left(\ln \left[\frac{8\pi^2 I k_{\text{B}} T}{\sigma h^2} \right] + 1 \right)$$

$$S_{\text{rot}}^{\text{non-linear}}(T) = k_{\text{B}} \left(\ln \left[\frac{\sqrt{\pi I_A I_B I_C} (8\pi^2 k_{\text{B}} T)^3}{\sigma h^3} \right] + \frac{3}{2} \right)$$

where σ is a symmetry number, I is the moment of inertia for a linear cluster and I_{A-C} are the principal moments of inertia for a non-linear cluster.^[13]

A cluster's symmetry number σ , corresponds to how many different, but indistinguishable, arrangements it has. The symmetry group, and thereby also σ is automatically determined by DMol³ in the free energy calculations. In some cases an incorrect σ might be determined by the program but the effect on the free energy is quite small. If DMol³ determines the symmetry number to be σ_{DMol} , but the actual symmetry number is σ_{DMol} the error becomes:

$$G_{\text{DMol}} - G_{\text{real}} = -k_{\text{B}} T \ln \left(\frac{\sigma_{\text{real}}}{\sigma_{\text{DMol}}} \right). \quad (2.15)$$

If σ_{real} is twice as large of what DMol³ determined the calculated free energy would be 18 meV to low at room temperature.

$E_{\text{vib}}, S_{\text{vib}}$. To determine the vibrational contributions to the enthalpy and entropy we approximate the vibrational modes of our clusters as quantum mechanical harmonic oscillators. Under this approximation the vibrational terms can be calculated as:

$$E_{\text{vib}} = \sum_{i=1}^d h\omega_i \left(\frac{1}{2} + \frac{1}{e^{h\omega_i/k_{\text{B}}T} - 1} \right)$$

$$S_{\text{vib}} = \frac{1}{T} \sum_{i=1}^d \left(\frac{h\omega_i}{e^{h\omega_i/k_{\text{B}}T} - 1} - k_{\text{B}} T \ln \left(1 - e^{-h\omega_i/k_{\text{B}}T} \right) \right)$$

where ω_i are the vibrational frequencies and d is the number of vibrational degrees of freedom.^[13] For a N -atom cluster we have $d = 3N - 5$ if it is linear and $d = 3N - 6$ if it is not. The first term in the energy expression is the vibrational energy of the lowest lying modes, often referred to as the zero-point energy.

To calculate the vibrational frequencies we need to determine how the forces acting on one atom depends on the positions of the other atoms. We can do this by constructing the following matrix:

$$M_{ij} = \frac{1}{\sqrt{m_i m_j}} \frac{\partial F_i(r_1, \dots, r_{3N})}{\partial r_j} \quad (2.16)$$

where r_i is a Cartesian coordinate of an atom, F_i is the corresponding force component and m_i is the mass of that atom. The vibrational frequencies are then the square roots of the eigenvalues of this matrix.^[14] The forces can be calculated through DFT but the derivatives have to be approximated. We do this by moving each atom independently, calculating new electronic forces each time. Each atom will be moved a distance d twice for each dimension, once in the negative direction and once in the positive direction. This makes it possible to approximate the derivatives through finite differences:

$$\frac{\partial F_i(r_1, \dots, r_{3N})}{\partial r_j} \approx \frac{F_i(\dots, r_j + d, \dots) - F_i(\dots, r_j - d, \dots)}{2d}.$$

In this thesis $d = 5 \text{ m\AA}$ is used. For the single-point calculations needed for the vibrational frequencies the spin is fixed to the lowest lying spin state.

S_{elec} . If the total spin state of the system is known the electronic entropy term can be calculated as: $k_B \ln(\text{spin degeneracy})$.^[13] For singlet states the spin degeneracy is one, for doublet states it is two and so on.

The many approximations made for the free energy calculations might give low precision when used to predict properties of our system at specific temperatures. However, conclusions about qualitative characteristics can still be valid.

2.7 Computational Method

DMol³ version 7.0 was used to perform electronic structure calculations from first principles. All calculations were performed using the PBE^[12] exchange-correlation functional. The basis used was dnp^[15], a local double numerical basis set with polarization functions. A cutoff value of 5 \AA was used for all basis functions. To reduce computational cost, the 10 lowest orbitals for copper were described using density functional semi-core pseudopotentials (DSPP)^[16]. The resulting basis set is shown in Table 2.1. The minimal basis set contains one orbital for each pair of principal and azimuthal quantum number present in the atom. The primed orbitals (double) adds an additional radial part to that orbital while the extra polarization orbitals adds more variation to the angular part of the wave functions. In Table 2.2 the difference between spin-polarized and non spin-polarized calculations for low energy copper oxide clusters is shown. It seems there is a risk that running restricted calculations for the GA simulations will change the internal ordering of the clusters

Table 2.1: The table shows the basis sets describing the electronic wave functions in the DFT calculations for oxygen and copper. All orbitals shown for each element were used.

	Minimal	Double	Polarization	Active electrons
O	1s 2s 2p	2s' 2p'	3d	8
Cu	3s 3p 3d 4s	3d' 4s'	4p	19

Table 2.2: Low energy Cu_nO_2 clusters^[17] were relaxed using spin-restricted calculations. After this a single-point unrestricted calculation was performed. The resulting total energy value, relative to the restricted value, is reported in the table (Single-point). Finally the clusters were relaxed using unrestricted calculations and the resulting total energy value, also relative to the restricted value, is reported in the table (Relaxed). All calculations used a smearing value of ≈ 0.25 eV (9 mHa). The Cu_3O_2 clusters were in a doublet state and the other clusters were triplets.

(meV)					
Single-point	-132	-10	-3	-38	-6
Relaxed	-136	-12	-3	-40	-7

and thereby make the simulation converge towards a different minimum. Therefore, as the computational time was not a problem, all DFT calculations were run using unrestricted spin. However, if larger clusters were to be investigated, using spin restricted calculations during the structure optimization in the GA simulation would be worth considering. To obtain a more accurate ground state energy the structure optimization could be followed by a spin unrestricted single point calculation.

For the GA simulation a smearing value of 0.25 eV was used (9 mHa) to aid convergence. The majority of the other calculations were run without smearing. In the cases where it was necessary to use smearing for convergence it is noted in the text.

3

Optimization

In the previous chapter we calculated the ground state electronic energy for fixed nuclei. However, we had no way of knowing if the nuclear positions we chose corresponded to a physically relevant structure of the system. Even if we use experimental values for our atomic structures there is no guarantee that these will correspond to the ground state structures in our simulations. This chapter will explain how the energy minima with respect to nuclear positions can be found for our system. First the case of local minima is treated. After this, it is shown how a GA can be used to find the global minimum structure.

3.1 Local Structure Optimization

According to the Hellmann-Feynman theorem, the forces acting on the nuclei of our system can be determined from the electron density using classical electrostatics.^[18] If we minimize these forces we will get closer to a stable structure. Changing the positions of the nuclei will, however, affect the electronic structure. By alternating DFT calculations and force calculations/minimizations we will hopefully converge towards a local minimum of the structure. Some common quantities to consider when determining if a system is converged are: change in energy between iterations, change in positions of the nuclei between iterations and remaining forces acting on the nuclei.

Computational Method. The structures were optimized using DMol³'s built in optimizer. For the GA simulations DMol³'s default settings were used, see GA column in Table 3.1. The structure optimizations were run for 200 iterations or until the energy convergence criteria and either the displacement or gradient criteria was satisfied. Structures which had not converged after 200 iterations were still used by the GA. A maximum of 50 SCF-iterations were allowed. If the SCF had not converge by then the structure optimization continued regardless.

For structure optimizations outside of the GA more accurate settings were used, see non-GA column in Table 3.1. The structures were considered relaxed when all convergence criteria were satisfied simultaneously.

Table 3.1: The table shows the settings used for local structure optimizations, both for GA simulations and outside them (non-GA). The integration grid setting controls the number of grid points used. Below this the three convergence settings are shown. The first two concerns the maximum allowed change in properties in between DFT calculations. The two properties are change in energy, and change in position of the nuclei, respectively. The last convergence setting defines the maximum allowed force component after a force calculation.

	GA	non-GA
Integration_Grid	medium	fine
Opt_Energy_Convergence (meV)	0.27 (10^{-5} Ha)	0.20
Opt_Displacement_Convergence (mÅ)	0.53 ($10^{-3} a_0$)	0.53
Opt_Gradient_Convergence (meV/Å)	50	2

3.2 Global Structure Optimization

Atomic clusters can have many different stable configurations, i.e. structures which are local minima with respect to energy. These can be found using the local optimization described in the previous section. Which minimum the local optimizer finds depends on the initial coordinates of the cluster. Finding the local minimum with the lowest energy, i.e. the global minimum, can be challenging. In this thesis a global optimizer based on a genetic algorithm (GA) was used to accomplish this. The algorithm generates educated guesses for the initial positions of our cluster. These positions will then be passed to the local optimization algorithm. This section will start with a general description of GAs followed by an explanation of the implementation used in this thesis.

3.2.1 Genetic Algorithms

GAs are a type of global optimization method inspired by how organisms evolve through natural selection. In Wahde 2008^[19] a detailed description of GAs and their implementation is given. A short summary of some important concepts follows.

Fitness: A property which can be evaluated for all candidates and assumes its maximum value for the global optimum.

Initialization: Creating a random starting population. The initial population should be diverse in order to avoid premature convergence.

Mutation: Alters a candidate in some way. This operation often contains stochastic elements. Mutations adds diversity to a population.

Pairing: Characteristics of two previous candidates is used to create a new one. Pairing allows the algorithm to make large “jumps” in configuration space.

Selection: Selecting candidates from a population which are used to construct a new candidate. Candidates with high fitness have a larger probability of being chosen. This focuses the search towards parts of configuration space corresponding to high fitness.

A GA is stochastic; simulations which are started with identical input, can give different results. However, it is not a completely random search. Information from previous candidates is used to create new ones. Previous candidates with high fitness are chosen with higher probability than those with low. If implemented well this results in a much more efficient search through the configuration space than a random search would.

Compared to many traditional algorithms the definition of a GA is quite wide. The implementation can differ a lot depending on the investigated system. For example, constraints can be considered in different ways. One way is to punish systems which do not satisfy the constraints when calculating the fitness, another is to modify the GA operators to only generate candidates which do satisfy the constraints.

3.2.2 Local Implementation

In this section the GA implementation used for this thesis is presented. A non-generational GA available in ASE^[20] was used. An overview of the algorithm looks as follows:

1. Generate and relax the initial population.
2. Generate a new candidate.
3. Relax the new candidate.
4. Has the simulation converged?
 - Yes → Finished! Go to step five.
 - No → Generate new population and return to step two.
5. Relax the unique top candidates using more accurate settings.

A more detailed explanation of the steps is given below.

Step 1. In the first step candidates with random structures are generated and relaxed using the structure optimization described in Section 3.1. These candidates make up the initial population.

Step 2. When an initial population exists it is possible to generate new candidates from it. A new candidate is generated through either pairing of two previous candidates (70% chance), or mutation of one previous candidate (30% chance). The optimal pairing-mutation ratio was suggested to be 66%–80% by Lysgaard^[21].

The probability that candidate i is chosen for pairing or mutation depends on its energy (E_i), the number of times it has been selected for pairing before (n_i), and the number of similar candidates (m_i). It is calculated as $F_i \cdot U_i$ where the two factors are defined as:

$$F_i = \frac{1}{2} [1 - \tanh(2\rho_i - 1)], \quad \rho_i = \frac{E_i - E_{\min}}{E_{\max} - E_{\min}} \quad (3.1)$$

$$U_i = \frac{1}{\sqrt{1 + n_i}} \cdot \frac{1}{\sqrt{1 + m_i}}. \quad [22]$$

Here, E_{\min} and E_{\max} are the lowest and highest energies in the population, respectively.

The pairing operator was developed by Deaven and Ho^[23]. It works as follows. First a randomly oriented plane containing the center of mass of each cluster is generated. Then a new cluster is constructed using atoms from different sides of the plane for each parent cluster. The plane is moved along a line perpendicular to it in order to get the correct number of atoms. If the atomic composition is wrong after this it is restored by randomly choosing an atom of a abundant type and changing it to an atom type of which there are too few. If any atoms from the different clusters has ended up too close to each other the halves are separated.

For the pure copper clusters two different mutation operators are used: mirror and rattle. For the copper oxide clusters a permutation mutation is used as well. All of them are available in ASE. Each mutation operator has an equal probability of being used. They work as follows. The **mirror mutation** generates a randomly oriented plane, splitting the cluster in half. One of the halves is replaced by the mirror image of the other. If the **rattle mutation** is chosen each atom has a 40% chance of being rattled. Being rattled means the atom is moved a random distance of up to 0.8 Å along each axis. If it ends up too close to another atom a new rattle operation, starting from the original position, is performed. The **permutation mutation** switches the positions of two atoms of different type. This is done $\lceil \text{number of atoms}/6 \rceil$ times.

Step 3. Here the new candidate is relaxed using the local structure optimization. In successive steps this candidate is included in the population if it has low enough energy and no similar candidates already exist. To determine if two clusters are similar the `InteratomicDistanceComparator` class provided in the `ase.ga` module is used. A maximum relative accumulated distance of 0.015, a maximum value difference of 0.7 Å and a maximum energy difference of 0.02 eV are used for the comparator. An explanation of these parameters is provided by Vilhelmsen et al.^[24].

Step 4. In the forth step of the algorithm a convergence check is made. Typically, one checks if any of the top candidates have changed for the last iterations.^[21] If the simulation had not converged a new population is constructed. This consists of the non-similar individuals with the lowest energy.

Step 5. To reduce computational time the local optimizations in the GA are run using the less accurate “GA” settings in Table 3.1. After the GA has finished the global minimum then has to be relaxed using the more accurate “non-GA” settings. As the top candidates can be close in energy several of them are relaxed using these settings. The candidate having the lowest energy computed with the accurate settings is considered the global minimum.

There are some additional GA features which potentially could work well for copper oxide structures, but which have not been implemented in this thesis. Two examples are screening and a spin mutation operator, both discussed below.

Screening. Screening could be used to decrease the runtime of the GA. Before a new candidate is relaxed the algorithm checks if a similar candidate has been relaxed before. If this is the case the previous relaxation result could be used for this candidate as well. It would of course take some tuning to get this to work properly.

Spin mutation. The spin mutation would remove the need for converging the spin state of the system. For DFT calculations, the spin state can be chosen by fixing the number of unpaired electrons. By having a mutation operator which randomly assigns the number of unpaired electrons, the SCF loops in the relaxation might converge faster. However, some fixed spin states could also hinder converges. Before implementing such an operator, a more thorough investigation should be made of how fast a system with a randomly chosen spin state converges compared to the unrestricted case.

4

Results

In the first part of this chapter the results from local structure optimizations on copper oxide clusters are presented and compared to previous theoretical work. It is found that the results of this thesis are largely consistent with previous findings.

The second part contains the results from global structure optimizations. These are compared to both experimental and theoretical work. When comparing to experimental results several experimentally found trends are reproduced theoretically. In the comparison to previous theoretical findings a functional dependence is found for the global minimum structures.

All visualizations of clusters for the figures and tables were made using OVITO^[25].

4.1 Local Structure Optimization

In order to produce accurate and efficient results using the global optimization algorithm the local optimization has to perform well. To ensure this, some calculations were compared to the results of two articles which also investigate small oxidized copper clusters using DFT. In the article by Trinchero et al.^[26] the same exchange correlation functional, basis set, real space cutoff and pseudopotential as in this thesis were used. The same convergence criteria for the structure optimization were used as well. Yuan et al.^[17] also used the PBE functional. However, they did use a different basis set, namely an all electron basis set of 20 primitive Gaussians.

4.1.1 Molecular Adsorption

Adsorption of one oxygen molecule on copper clusters was investigated and compared to previous theoretical work, see Table 4.1. The adsorption energy is defined as

$$E_{\text{ad}} = E(\text{O}_2) + E(\text{Cu}_n) - E(\text{Cu}_n\text{O}_2), \quad (4.1)$$

where $E()$ gives the ground state energy of the systems. The calculated adsorption energies are similar to previous results. In all but one case the energy difference is below 0.1 eV. The bond lengths of the adsorbed oxygen molecules are presented as well. The results agree well with earlier findings, in all cases the difference is less than 0.01 Å. The bond length can give hints of the charge state of the oxygen atoms. For gas phase O_2 , O_2^- and O_2^{2-} the bond lengths were calculated to be 1.225 Å, 1.379 Å and 1.686 Å, respectively.

Table 4.1: The table shows results for molecular adsorption of oxygen on the lowest energy structures of Cu_{2-4} and Cu_6 . The resulting clusters are shown and the corresponding adsorption energies (E_{ad}) are reported in eV and compared to earlier results ($E_{\text{Trincherro}}$, E_{Yuan}). For Cu_2 and Cu_3 a second low energy structure is included as well. Bond lengths for the adsorbed oxygen molecules (O_{bl}) are also shown. The values in parenthesis are differences from the values calculated by Yuan et al.^[17]. In all cases, the calculations resulted in the same spin multiplicities (Spin) as in previous work.

	E_{ad}	$E_{\text{Trincherro}}^{[26]}$	$E_{\text{Yuan}}^{[17]}$	O_{bl} (Å)	Spin
	0.81	-0.16	-0.08	1.276 (+0.005)	triplet
	0.29	N/A	+0.00	1.366	triplet
	2.00	N/A	-0.06	1.367 (+0.008)	doublet
	1.63	N/A	-0.03	1.344	doublet
	1.22	+0.04	-0.01	1.366 (+0.006)	triplet
	1.32 (1.63 $^\alpha$)	+0.05	+0.03 $^\alpha$	1.500 (+0.003)	singlet

$^\alpha$ These values are calculated with a reference energy from the to the 3-D C_{2v} Cu_6 isomer instead of the lowest lying 2-D C_{3v} one. Both are shown in Table A.1.

4.1.2 Bulk Stoichiometry

Here clusters with the same stoichiometry as cuprous oxide (Cu_2O) are investigated. In Table 4.2 formation enthalpies of $(\text{Cu}_2\text{O})_n$ clusters with n -values from one to six are compared to previous work by Trincherro et al.^[26]. The formation enthalpy is defined as

$$H_f = \frac{E(\text{Cu}_{2m}\text{O}_m)}{m} - \frac{E(\text{O}_2)}{2} - \frac{E(\text{Cu}_{2m})}{m}, \quad (4.2)$$

where $E()$ gives the ground state energy of the systems. Except for Cu_4O_2 the calculated values in this thesis were 0.10–0.15 eV higher. The most stable electronic structure of Cu_4O_2 was determined to be a singlet state by Trincherro et al. as opposed to the triplet state found in this thesis. The spin states of the other clusters were not reported.

The effect of changing the charge of a cluster was also briefly explored. In Table 4.3 results for Cu_2 clusters are shown, both in the bare copper case and with one oxygen atom adsorbed. In both cases the energy was affected more by removing one electron than by adding one. For the oxide the angle between the Cu-O bonds increased significantly by removing one electron while it was barely affected when one electron was added.

Table 4.2: The table shows enthalpy of formation for $(\text{Cu}_2\text{O})_n$ clusters with n -values from one to six. A comparison to previous work is made as well. For the Cu_6O_3 cluster a smearing value of ≈ 10 meV (0.5 mHa) was used. No smearing was used when calculating the other energies.

(eV)						
H_f^α	-1.14	-1.79	-1.90	-2.05	-2.27	-2.31
$H_{\text{Trincherro}}^\beta$	-0.12	-0.03	-0.10	-0.11	-0.15	-0.15
Spin	singlet	triplet	triplet	singlet	singlet	singlet

^{α} Enthalpy of formation in eV. The values are calculated with respect to the lowest lying bare clusters in Table A.1 and gas phase O_2 .

^{β} Shows how previous results^[26] differs from the results of this thesis (in eV).

Table 4.3: In the table properties for Cu_2 and Cu_2O clusters with charge of -1 , 0 or $+1$ (q) are compared. The bond length (B.L.) is the distance between the copper atoms and the angle is between the Cu-O bonds. All neutral systems were found to be singlets and the charged systems were doublets.

q	Cu_2			Cu_2O			
	B.L. (Å)	$\Delta_{\text{H-L}}^\alpha$	E_{rel}^β	B.L. (Å)	Angle	$\Delta_{\text{H-L}}^\alpha$	E_{rel}^β
1	2.38	0.33	8.23	3.19	128.6°	0.38	7.90
0	2.26	1.57	0.00	2.53	90.7°	1.16	0.00
-1	2.43	0.79	-0.53	2.57	90.1°	0.58	-0.89

^{α} HOMO-LUMO gap (eV).

^{β} Energy relative neutral cluster (eV).

4.2 Global Structure Optimization

This section contains results related to global structure optimization. First some statistics for the genetic algorithm (GA) is presented. After this, free energies are compared to investigate the stability of copper oxide clusters at different temperatures. Some of the results are also compared to experiments. In the end of the section a comparison to previous theoretical results for the global minima of $\text{Cu}_{1-3}\text{O}_{1-6}$ clusters is made.

4.2.1 Statistics $[\text{Cu}_6\text{O}_{3,6}]^-$

In order to get a better understanding of the GA's performance, two systems of different size, $[\text{Cu}_6\text{O}_3]^-$ and $[\text{Cu}_6\text{O}_6]^-$, were more thoroughly investigated. Each system was evaluated 50 times by the GA. The simulations ran for 100 steps or until the global minimum was found. An overview of the result can be seen in Figure 4.1. The solid lines show how the algorithm performs on average. The dotted lines show the performance of worst run, i.e. the one with the highest final

4. Results

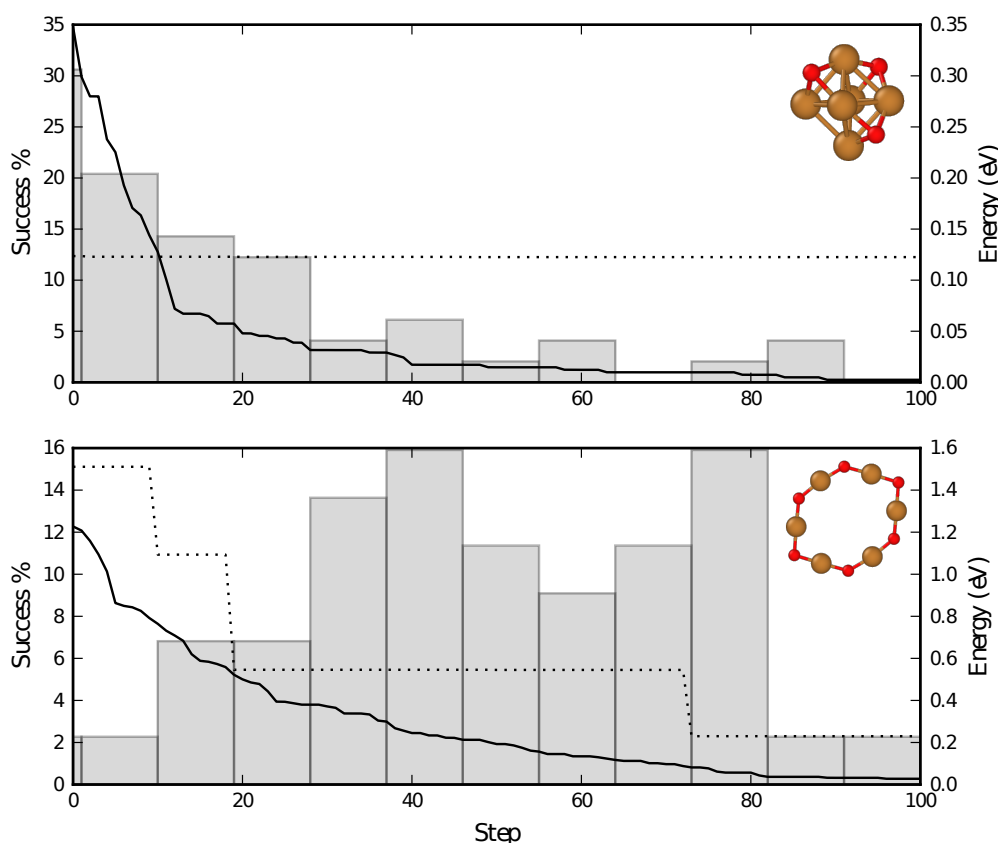


Figure 4.1: In the figure statistics for $[\text{Cu}_6\text{O}_3]^-$ (top) and $[\text{Cu}_6\text{O}_6]^-$ (bottom) are shown. Each cluster was optimized 50 times by the GA using a population size of 15. The histograms show for which step the successful GA runs first found the global minimum. They are associated with the values on the left axis. The narrow box at step zero contains all runs where the global minimum existed already in the initial population. The dotted line shows the energy of the best candidate at each step, in the run resulting in the highest final energy. The solid line shows the average energy of the best candidates from all runs. Both lines are associated with the values on the right axis. The energies are relative the global minima.

energy. In both cases the energy of the best candidate is considered at a specific step.

The histograms in Figure 4.1 shows for which steps the minimum was found. In the $[\text{Cu}_6\text{O}_3]^-$ case the algorithm often finds the minimum early. The fact that about 30% of the initial populations contained the minimum also indicates that this minimum is found quite easily. In order to find the $[\text{Cu}_6\text{O}_6]^-$ minimum the algorithm has to do more work. It is not as likely that the final candidate can be generated directly from the initial population. Therefore, intermediate candidates are needed more often. These are on average closer in energy to the final candidate than a randomly generated population is.

Additional information for these simulations is shown in Table 4.4. The extra atoms in $[\text{Cu}_6\text{O}_6]^-$ compared to $[\text{Cu}_6\text{O}_3]^-$ make the local optimization, which is the major contribution to the execution time, considerably slower. As the larger system also

has a lower success rate and on average needs a significantly larger amount of steps to find the minimum, the run time of the algorithm quickly increases with increased system size.

Table 4.4: *Further information about the GA runs in Figure 4.1. The success rate is the ratio of runs which have found the global minimum within 100 steps. Steps to minimum is the average amount of steps needed for a successful run to encounter the global minimum. How long time it takes on average to construct, relax, and add a new candidate in the GA is referred to as time/step. The corresponding time for the randomly generated initial candidates is referred to as time/initial candidate. The initial mean energy is the mean energy of all initial randomly generated candidates. Minimum from random is the proportion of randomly generated candidates resulting in the global minimum. All time measurements are expressed as wall clock time \times number of CPUs used.*

	$[\text{Cu}_6\text{O}_3]^-$	$[\text{Cu}_6\text{O}_6]^-$
Success rate	98%	88%
Steps to minimum	18	49
Time/step (h)	1.5	6.9
Time/initial candidate (h)	1.9	7.4
Initial mean energy (eV)	2.9	5.0
Minimum from random	2.40%	0.13%

4.2.2 Stability of Copper Oxide Clusters

The stability of copper oxide clusters was investigated. This was done by comparing the free energy of bare copper clusters and gas phase oxygen molecules to the free energy of oxidized clusters. Neutral as well as singly charged clusters were studied. The neutral ones were composed of one to three copper atoms and one to six oxygen atoms; the charged ones were composed of six copper atoms and three to nine oxygen atoms. The ground state structures of the oxidized clusters are shown in this section as well.

The stability was investigated at three different temperatures. The two lower, 298 K and 573 K, are the temperatures for which the experiments by Morita et al.^[3] were performed. The top temperature, 1517 K, corresponds to the melting temperature of bulk cuprous oxide.^[27]

$\text{Cu}_{1-3}\text{O}_{1-6}$. In Figure 4.2 the change in free energy for forming $\text{Cu}_{1-3}\text{O}_{1-6}$ clusters from the corresponding bare copper cluster, see Table A.1, and gas phase oxygen molecules is shown. The structures of the oxides are shown in the figure as well. Many of the oxygen-rich clusters have a low free energy for the two lower temperatures. At 1517 K all clusters with $n = 1$ or $n = 2$ are predicted to decompose except Cu_2O . Clusters containing three copper atoms are only predicted to decompose in the cases of five or six oxygen atoms. Those with fewer oxygen atoms are all predicted to be stable. Specifically, the clusters with one, two or four oxygen atoms lower their free energy with about 0.7 eV and Cu_3O_3 lowers it by 1.85 eV.

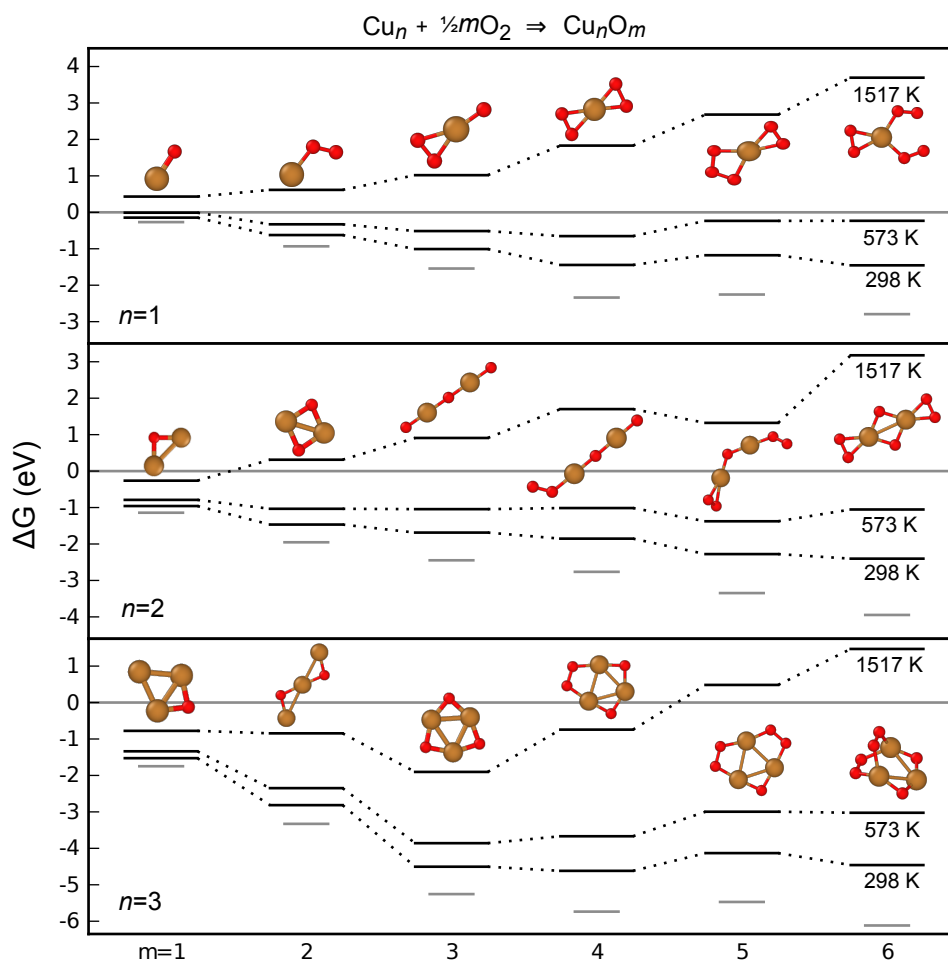


Figure 4.2: The black lines show the change in free energy at three different temperatures for the reaction at the top figure. Formation enthalpies are included as well (gray lines). The case of one, two and three copper atoms are considered in the top, middle and bottom part of the figure respectively. The number of oxygen atoms in the clusters varies from one two six. The respective global minimum structures for the different compositions are also shown.

$[\text{Cu}_6\text{O}_{3-9}]^{+/-}$. As seen in Table 4.3, changing the charge of a cluster can alter its structure. Therefore, separate global optimizations were performed for the differently charged clusters. The resulting structures for the $\text{Cu}_6^{+/-}$ clusters are shown in Table A.3 and the structures for $[\text{Cu}_6\text{O}_{3-9}]^{+/-}$ are shown in Figure 4.3.

The $[\text{Cu}_6\text{O}_{3-9}]^{+/-}$ clusters have previously been investigated experimentally, see Figure 1.1. In Figure 4.3 the relevant experimental results are included on the right hand side of the figure. The figure also shows the change in free energy for forming the clusters at different temperatures. In general the free energy gain is larger for the anions than for the cations. At the two lower temperatures many clusters are quite close in energy. For example, the $[\text{Cu}_6\text{O}_{4-6,8}]^+$ clusters all lie in an interval of 100 meV at 298 K and the $[\text{Cu}_6\text{O}_{4,5,7}]^+$ clusters lie within 125 meV of each other at 573 K.

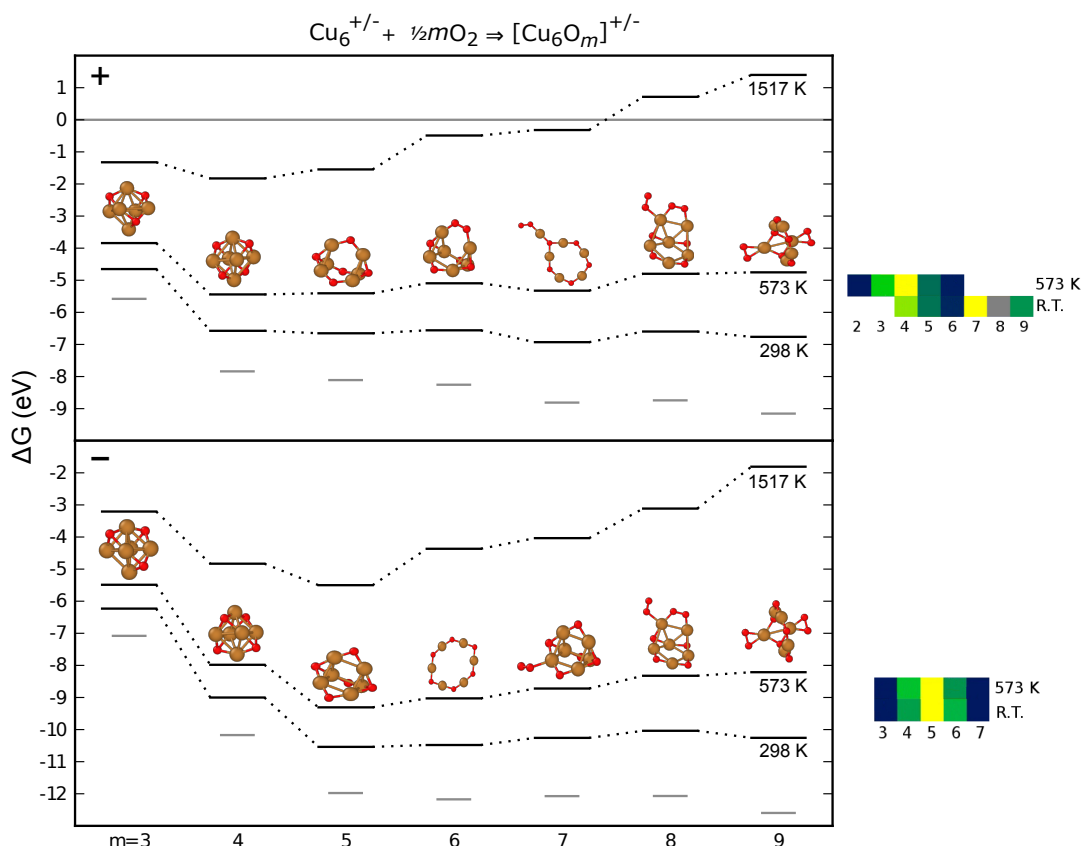


Figure 4.3: The black lines show the change in free energy at three different temperatures for the reaction at the top figure. Formation enthalpies are included as well (gray lines). The clusters are composed of six copper atoms and three to nine oxygen atoms. Cations are shown in the top part of the figure and anions are shown in the bottom part. The respective global minimum structures for the different compositions are also shown. Experimental results for the relative abundances of the different clusters are included as heat maps on the right hand side of the figure. Two different temperatures are considered, room temperature and 573 K. The heat maps were extracted from Figure 1.1 (adapted with permission from Morita et al.^[3]. Copyright 2013 American Chemical Society).

It is possible to identify some trends regarding the stability. Several of them are similar to the experimental ones. For the cations the following similarities are observed:

- $[\text{Cu}_6\text{O}_7]^+$ is most stable composition at 298 K.
- $[\text{Cu}_6\text{O}_4]^+$ becomes the most stable composition at high temperatures.
- $[\text{Cu}_6\text{O}_6]^+$ and $[\text{Cu}_6\text{O}_8]^+$ are unlikely to exist.
- $[\text{Cu}_6\text{O}_9]^+$ is unlikely to exist at high temperatures.

Similarities exist for the anions as well:

- $[\text{Cu}_6\text{O}_5]^-$ is most stable from 298 K and up.
- $[\text{Cu}_6\text{O}_6]^-$ is more stable than $[\text{Cu}_6\text{O}_4]^-$ at 298 K.
- $[\text{Cu}_6\text{O}_4]^-$ becomes more stable than $[\text{Cu}_6\text{O}_6]^-$ at higher temperatures.

There are also some characteristics of the theoretical data which do not agree with experiments:

- $[\text{Cu}_6\text{O}_3]^+$ is unlikely to exist at 573 K.
- $[\text{Cu}_6\text{O}_4]^-$ is unlikely to exist except for very high temperatures.
- $[\text{Cu}_6\text{O}_9]^-$ could exist at 298 K.

4.2.3 Previous Results $\text{Cu}_{1-3}\text{O}_{1-6}$

There have been previous attempts of finding the ground state structures of $\text{Cu}_{1-3}\text{O}_{1-6}$ clusters^[28-34]. These structures were compared to the structures found in this thesis. Several of the previous studies did not optimize the spin state of the clusters. Therefore the spin state was not considered when determining if the results of different studies agreed or not. Exact bond lengths and angles were not considered either, only the general shape of the clusters was compared. In some cases the result was the same or similar to that of this thesis, in other cases different structures were found. A summary is shown in Table 4.5.

Table 4.5: Comparing global minimum structures with previous theoretical work. In some cases the same ground state structure was found (Agree), in others a different structure was found (Disagree). Bae^[34] used multiple Monte Carlo simulations starting from different initial structures to determine the optimal structure. In the other articles different structures were compared manually. Different exchange-correlation functionals were used in the articles; these are show in the table (E_{xc}).

Authors	Year	Agree	Disagree	E_{xc}
Wang et al. ^[28]	1996	$\text{Cu}_2\text{O}_{1,2}$	Cu_2O_4	BLYP
Chertihin et al. ^[29]	1997	CuO_{2-4} , $\text{Cu}_2\text{O}_{1,3}$	Cu_2O_2	B3LYP
Baruah et al. ^[30]	2004	$\text{CuO}_{2,3,6}$	N/A	PBE
Pouillon et al. ^[31]	2004	CuO_{3-5}	$\text{CuO}_{2,6}$	PW91
Dai et al. ^[32]	2004	$\text{Cu}_2\text{O}_{1,3,4}$	Cu_2O_2	BLYP, B3LYP
Gong et al. ^[33]	2009	$\text{CuO}_{4,5}$	N/A	B3LYP
Bae. ^[34]	2016	$\text{Cu}_3\text{O}_{3-5}$	$\text{Cu}_3\text{O}_{1,2,6}$	B3LYP

If different structures had been found they were investigated further. The structures were relaxed using same implementation of DFT that the clusters in this thesis used. In all cases this resulted in energies close to those for the global minima found in this thesis, see Table 4.6.

Table 4.6: The table shows the energy of ground state structures found in other articles relative the energy of the most stable structures found in this thesis (E_{diff}). The energies are obtained after relaxing the systems described in the articles using settings covered in sections 2.7 and 3.1. The obtained spin multiplicity (Spin) is shown as well. It can take the value singlet (s), doublet (d) or triplet (t).

		E_{diff} (eV)	Spin			E_{diff} (eV)	Spin
	CuO_2 ^[31]	0.41 eV	d		Cu_2O_4 ^[28]	0.09 eV	s
	CuO_6 ^[31]	0.75 eV	d		Cu_3O ^[34]	0.19 eV	d
	Cu_2O_2 ^[29]	0.16 eV	t		Cu_3O_2 ^[34]	0.16 eV	d
	Cu_2O_2 ^[32]	0.26 eV	t		Cu_3O_6 ^[34]	1.03 eV	d

5

Conclusion

The most stable structures of copper oxide clusters were determined using a genetic algorithm (GA). Implementing and testing the GA was part of this thesis and the results regarding its performance could be useful in other global structure optimizations. Below, conclusions both regarding the GA performance and for the copper oxide clusters are presented.

5.1 Genetic Algorithm

For the smaller clusters, around nine atoms or less, the search space is too small for the GA operations to do any major contributions the optimization. For example, a randomly generated $[\text{Cu}_6\text{O}_3]^-$ cluster had a 2.4% chance of being the global minimum. On average, 42 random candidates would thereby contain one global minimum. Using the GA, 15 initial candidates plus 18 steps (33 local optimizations) were needed on average to find one global minima.

For the larger cluster ($[\text{Cu}_6\text{O}_6]^-$) the GA operations were of greater importance. Of the 750 random candidates, only one was relaxed to the global minimum. However, on average the GA only needed 15 + 49 local optimizations to find the minimum. As a local optimization performed in a GA step on average was faster than a local optimization performed on a randomly generated candidate, the improved computational time is even better than that indicated by the number of steps saved.

Overall the implementation of the DFT and GA used in this thesis seems to be a good compromise between accuracy and computational cost. It is accurate enough to reproduce experimental results while keeping execution time at a manageable level.

Outlook. Comparing the GA to a random search can show if the algorithm was implemented in a sane way. However, a more fair comparison of its performance would be to compare it to other global structure optimization algorithms used today, such as basin hopping. This is a possible focus for future work on the subject.

5.2 Copper Oxide Clusters

The results for the copper oxide clusters can be divided in to two cases: local and global structure optimization. In the pure local optimization case, several earlier results for formation enthalpies and adsorption energies were reproduced. This created a good starting point for the global optimization as the local optimization is an important part of the GA. The results from the global optimization are considered below.

Cu₁₋₃O₁₋₆. Many of the oxygen-rich clusters had a low free energy at room temperature and at 573 K. Only considering formation enthalpies, the clusters containing six oxygen atoms were the most stable ones. From the comparison with previous studies it is concluded that the global minima depends on the exchange-correlation functional used. However, in the cases where the minima of different functionals did not match, they were still close in energy when compared using the PBE functional.

[Cu₆O₃₋₉]^{+/-}. For the charged clusters several trends found experimentally by Morita et al.^[3] were reproduced theoretically. For example, the most stable compositions, both at room temperature and at high temperatures, agreed with experiments.

In the free energy comparisons only the most stable structures of the clusters were considered. However, as seen in Figure A.1, several structures with only slightly higher energies (within 1 eV) can exist. For a more complete picture of the system, these structures could be considered as well.

Outlook. The functional dependence of the global minima was only briefly explored. A more systematic investigation, combined with a comparison to experimentally determined structures, would help to get a better understanding of the clusters.

To get a better understanding of the connection between the calculated free energy values and the experimentally measured spectrum, it would be helpful to compare clusters containing a different number of copper atoms. A natural continuation would be to investigate other parts of the experimental results in Figure 1.1.

Bibliography

- [1] Feng Gao, Eric D. Walter, Nancy M. Washton, János Szanyi, and Charles H. F. Peden. Synthesis and Evaluation of Cu-SAPO-34 Catalysts for Ammonia Selective Catalytic Reduction. 1. Aqueous Solution Ion Exchange. *ACS Catalysis*, 3(9):2083–2093, 2013.
- [2] Sunney I. Chan, Yu-Jhang Lu, Penumaka Nagababu, Suman Maji, Mu-Cheng Hung, Marianne M. Lee, I-Jui Hsu, Pham Dinh Minh, Jeff C.-H. Lai, Kok Yoah Ng, Sridevi Ramalingam, Steve S.-F. Yu, and Michael K. Chan. Efficient Oxidation of Methane to Methanol by Dioxygen Mediated by Tricopper Clusters. *Angewandte Chemie International Edition*, 52(13):3731–3735, 2013.
- [3] Keisuke Morita, Kazuko Sakuma, Ken Miyajima, and Fumitaka Mafuné. Thermally and Chemically Stable Mixed Valence Copper Oxide Cluster Ions Revealed by Post Heating. *The Journal of Physical Chemistry A*, 117(40):10145–10150, 2013. PMID: 24004032.
- [4] Fumitaka Mafuné, Ken Miyajima, and Keisuke Morita. Release of Oxygen from Copper Oxide Cluster Ions by Heat and by Reaction with NO. *The Journal of Physical Chemistry C*, 119(20):11106–11113, 2015.
- [5] P.D. Haynes. *Linear-scaling methods in ab initio quantum-mechanical calculations*. PhD thesis, University of Cambridge, 1998.
- [6] M. Born and R. Oppenheimer. Zur Quantentheorie der Molekeln. *Annalen der Physik*, 389(20):457–484, 1927.
- [7] P. Hohenberg and W. Kohn. Inhomogeneous Electron Gas. *Phys. Rev.*, 136:B864–B871, Nov 1964.
- [8] W. Kohn and L. J. Sham. Self-Consistent Equations Including Exchange and Correlation Effects. *Phys. Rev.*, 140:A1133–A1138, Nov 1965.
- [9] J. Thijssen. *Computational Physics*. Cambridge University Press, 2nd edition, 2007.
- [10] M. Weinert and J. W. Davenport. Fractional occupations and density-functional energies and forces. *Phys. Rev. B*, 45:13709–13712, Jun 1992.
- [11] G. L. Oliver and J. P. Perdew. Spin-density gradient expansion for the kinetic energy. *Phys. Rev. A*, 20:397–403, Aug 1979.
- [12] John P. Perdew, Kieron Burke, and Matthias Ernzerhof. Generalized Gradient Approximation Made Simple. *Phys. Rev. Lett.*, 77:3865–3868, Oct 1996.
- [13] C.J. Cramer. *Essentials of computational chemistry: theories and models*. Wiley, 2nd edition, 2004.
- [14] E. B. Wilson, J. C. Decius, and P. C. Cross. *Molecular Vibrations*. Dover, New York, 1980.

- [15] B. Delley. From molecules to solids with the DMol3 approach. *The Journal of Chemical Physics*, 113(18):7756–7764, 2000.
- [16] B. Delley. Hardness Conserving Semilocal pseudopotentials. *Phys. Rev. Lett.*, 66:155125, 2002.
- [17] Xiuxiang Yuan, Liuxia Liu, Xin Wang, Mingli Yang, Koblar Alan Jackson, and Julius Jellinek. Theoretical Investigation of Adsorption of Molecular Oxygen on Small Copper Clusters. *The Journal of Physical Chemistry A*, 115(31):8705–8712, 2011. PMID: 21732667.
- [18] R. P. Feynman. Forces in Molecules. *Phys. Rev.*, 56:340–343, Aug 1939.
- [19] M Wahde. *Biologically inspired optimization methods: an introduction*, volume 1. WIT Press, 2008.
- [20] S. R. Bahn and K. W. Jacobsen. An object-oriented scripting interface to a legacy electronic structure code. *Comput. Sci. Eng.*, 4(3):56–66, May-Jun 2002.
- [21] Steen Lysgaard. *Computational analysis of gas-solid interactions in materials for energy storage and conversion*. PhD thesis, Technical University of Denmark, 2013.
- [22] Lasse B. Vilhelmsen, Krista S. Walton, and David S. Sholl. Structure and Mobility of Metal Clusters in MOFs: Au, Pd, and AuPd Clusters in MOF-74. *Journal of the American Chemical Society*, 134(30):12807–12816, 2012. PMID: 22734664.
- [23] D. M. Deaven and K. M. Ho. Molecular Geometry Optimization with a Genetic Algorithm. *Phys. Rev. Lett.*, 75:288–291, Jul 1995.
- [24] Lasse B. Vilhelmsen and Bjørk Hammer. A genetic algorithm for first principles global structure optimization of supported nano structures. *The Journal of Chemical Physics*, 141(4):044711, 2014.
- [25] Alexander Stukowski. Visualization and analysis of atomistic simulation data with OVITO the Open Visualization Tool. *Modelling and Simulation in Materials Science and Engineering*, 18(1):015012, 2010.
- [26] Adriana Trincherro, Simon Klacar, Lauro Oliver Paz-Borbón, Anders Hellman, and Henrik Grönbeck. Oxidation at the Subnanometer Scale. *The Journal of Physical Chemistry C*, 119(20):10797–10803, 2015.
- [27] "Physical Constants of Inorganic Compounds" in CRC Handbook of Chemistry and Physics, 97th Edition (Internet Version 2017), W. M. Haynes, ed., CRC Press/Taylor & Francis, Boca Raton, FL.
- [28] Lai-Sheng Wang, Hongbin Wu, Sunil R. Desai, and Liang Lou. Electronic structure of small copper oxide clusters: From Cu₂O to Cu₂O₄. *Phys. Rev. B*, 53:8028–8031, Mar 1996.
- [29] George V. Chertihin, Lester Andrews, and Charles W. Bauschlicher. Reactions of Laser-Ablated Copper Atoms with Dioxygen. Infrared Spectra of the Copper Oxides CuO, OCuO, CuOCuO, and OCuOCuO and Superoxide CuOO in Solid Argon. *The Journal of Physical Chemistry A*, 101(22):4026–4034, 1997.
- [30] Tunna Baruah, Rajendra R. Zope, and Mark R. Pederson. Molecular structures and vibrations of neutral and anionic CuO_x ($x = 1-3, 6$) clusters. *Phys. Rev. A*, 69:023201, Feb 2004.
- [31] Y. Pouillon and C. Massobrio. Structural and electronic properties of small CuO_m clusters. *Applied Surface Science*, 226(13):306 – 312, 2004. EMRS 2003

- Symposium F, Nanostructures from Clusters A. Perez, O. Puglisi.
- [32] Bing Dai, Li Tian, and Jinlong Yang. A theoretical study of small copper oxide clusters: Cu_2O_x ($x=14$). *The Journal of Chemical Physics*, 120(6):2746–2751, 2004.
- [33] Yu Gong and Mingfei Zhou. Formation and characterization of the CuO_5 , CuO_4 and CuO_4^- complexes in solid argon. *Phys. Chem. Chem. Phys.*, 11(39):8714–8720, 2009.
- [34] Gyun-Tack Bae. Structures and Electronic Properties of Cu_3O_n ($n = 16$) Clusters using ab initio Monte Carlo Simulations. *Bulletin of the Korean Chemical Society*, 37(5):638–642, 2016.

A

Appendix

In Section A.1 are properties for locally optimized clusters presented. Section A.2 contains properties for the global minima found by the GA. In both of these cases binding energies are calculated. The binding energy is defined as:

$$E_b = n E(\text{Cu}) + m E(\text{O}) - E([\text{Cu}_n\text{O}_m]^{+/0/-}), \quad (\text{A.1})$$

where $E()$ gives the ground state energy of the systems. Note that the energy of the free atoms is not affected by an eventual charge on the cluster. The effect of this is that positively charged clusters get a lower binding energy than the corresponding neutral ones as they have “lost” electrons. In the same way a negatively charged clusters get a higher binding energy compared to neutral clusters.

In Section A.3 are typical distributions of the top candidates generated by the GA shown. The investigated clusters are $[\text{Cu}_6\text{O}_3]^-$ and $[\text{Cu}_6\text{O}_6]^-$.

A.1 Local Minima

Binding energies for copper clusters acquired through local optimization are shown in Table A.1. The binding energy per atom increases with system size in all cases. All clusters obtain their lowest energy for the lowest spin state, i.e. doublet for Cu_3 and singlet for all other.

Table A.1: The table shows calculated binding energies (E_b) and HOMO-LUMO gaps ($\Delta_{\text{H-L}}$) for copper clusters used in previous work^[17,26]. The E_b/Cu values are binding energies per atom. The Cu_3 cluster is in a doublet state, all other clusters are singlets.

	E_b	E_b/Cu	$\Delta_{\text{H-L}}$	(eV)		E_b	E_b/Cu	$\Delta_{\text{H-L}}$	(eV)
Cu_2	2.10	1.05	1.57		Cu_6	10.50	1.75	0.47	
Cu_3	3.35	1.12	0.32		Cu_8	16.12	2.02	1.54	
Cu_4	5.94	1.48	1.00		Cu_{10}	20.87	2.09	1.06	
Cu_6	10.82	1.80	1.87		Cu_{12}	26.03	2.17	0.82	

The clusters were used for calculations of adsorption energies and formation enthalpies in Section 4.1. The Cu_2 and Cu_3 clusters were also used to calculate the free energy differences shown in Figure 4.2. With the exception of the 3D Cu_6 cluster, these are reported to be the most stable structures.^[17,26]

A.2 Global Minima

Here are properties for the global minima found by the GA presented. For every cluster the binding energy, free energy contribution at room temperature (G_{rt}), spin state and symmetry group is shown. The binding energy is defined in Equation A.1 and G_{rt} corresponds to the difference between the calculated total free energy at room temperature and the electronic energy. The symmetry group was determined by DMol³.

Table A.2 shows the results for the $\text{Cu}_{1-3}\text{O}_{1-6}$ clusters. In the table the binding energy increases with system size while the free energy contribution is 0.40–0.90 eV for all clusters. The estimated stability of these clusters is shown in Figure 4.2.

Table A.2: *The table shows properties for the most stable structures of $\text{Cu}_{1-3}\text{O}_{1-6}$ found by the GA. The structures with three or less atoms were determined manually; all larger structures were found using the GA. Spin refers to the spin multiplicity which takes the values singlet (s), doublet (d), triplet (t) or quadruplet (q). The corresponding structures are shown in Figure 4.2.*

(eV)	Cu				Cu ₂				Cu ₃			
	E_b	G_{rt}	Spin	SG	E_b	G_{rt}	Spin	SG	E_b	G_{rt}	Spin	SG
O	2.18	-0.58	d	$C_{\infty v}$	6.62	-0.68	s	C_{2v}	8.48	-0.81	d	C_1
O ₂	7.67	-0.62	d	C_s	10.81	-0.60	s	D_{2h}	13.44	-0.75	d	C_{2h}
O ₃	11.65	-0.63	q	C_{2v}	14.68	-0.56	s	$D_{\infty h}$	18.75	-0.74	q	C_1
O ₄	15.83	-0.50	d	D_{2h}	18.38	-0.65	t	C_1	22.61	-0.60	d	C_{2v}
O ₅	19.13	-0.55	q	C_{2v}	22.34	-0.72	t	C_1	25.72	-0.61	d	C_1
O ₆	23.04	-0.51	d	C_{2v}	26.32	-0.47	t	D_{2h}	29.75	-0.53	d	C_s

In Table A.3 the results for the bare $\text{Cu}_6^{+/-}$ clusters are shown. Different structures are obtained for the different charge states. The positively charged structure got the same shape as a neutral cluster while the negatively charged structure is close to that of an oxidized cluster composed of six copper atoms and three or four oxygen atoms. The clusters are used to calculate the free energy differences shown in Figure 4.3.

The results for the $[\text{Cu}_6\text{O}_{3-9}]^{+/-}$ clusters are shown in Table A.4. The majority of the clusters are in the lowest spin state (doublet). The exceptions are $[\text{Cu}_6\text{O}_3]^+$ and $[\text{Cu}_6\text{O}_4]^+$ which are in a quadruplet state. For $[\text{Cu}_6\text{O}_9]^-$ no spin state was determined. The estimated stability of these clusters is shown in Figure 4.3.

Table A.3: Binding energy (E_b) and free energy contribution at room temperature (G_{rt}), both in eV, are shown for the most stable structures of Cu_6^+ and Cu_6^- found by the GA. The symmetry group (SG) is shown as well. Both clusters presented in the table were in a doublet spin state.

Cu_6^+	E_b	G_{rt}	SG	Cu_6^-	E_b	G_{rt}	SG
	3.80	-1.08	C_{2v}		11.97	-0.96	D_{4h}

Table A.4: The table shows properties for the most stable structures of $[\text{Cu}_6\text{O}_{3-9}]^{+/-}$ found by the GA. Spin refers to the spin multiplicity which takes the values doublet (d) or quadruplet (q). The corresponding structures are shown in Figure 4.3.

(eV)	+1				-1			
	E_b	G_{rt}	Spin	SG	E_b	G_{rt}	Spin	SG
Cu_6O_3	19.52	-0.85	q	C_{3v}	29.55	-0.81	d	C_s
Cu_6O_4	25.16	-0.74	q	C_{2v}	36.02	-0.71	d	C_1
Cu_6O_5	28.88	-0.78	d	C_{2v}	40.70	-0.68	d	C_{2v}
Cu_6O_6	32.33	-0.77	d	C_s	44.78	-0.65	d	D_{2h}
Cu_6O_7	36.24	-0.82	d	C_s	48.06	-0.76	d	C_1
Cu_6O_8	39.57	-0.78	d	C_1	51.44	-0.78	d	C_1
Cu_6O_9	43.37	-0.77	d	C_s	55.21	-0.70	N/A^α	C_{2v}

^{α} For this cluster's structure optimization to converge a smearing value of ≈ 27 meV (1 mHa) was used. When doing this the last electron was split in half between the two spin channels.

A.3 Comparing Top Candidates

Many different structures are generated by the GA. The energy distribution of the top candidates for $[\text{Cu}_6\text{O}_3]^-$ and $[\text{Cu}_6\text{O}_6]^-$ is shown in Figure A.1. The $[\text{Cu}_6\text{O}_6]^-$ clusters are closer in energy. This could be explained by that an increased number of atoms gives a higher number of possible configurations, making the energy difference between adjacent configurations less.

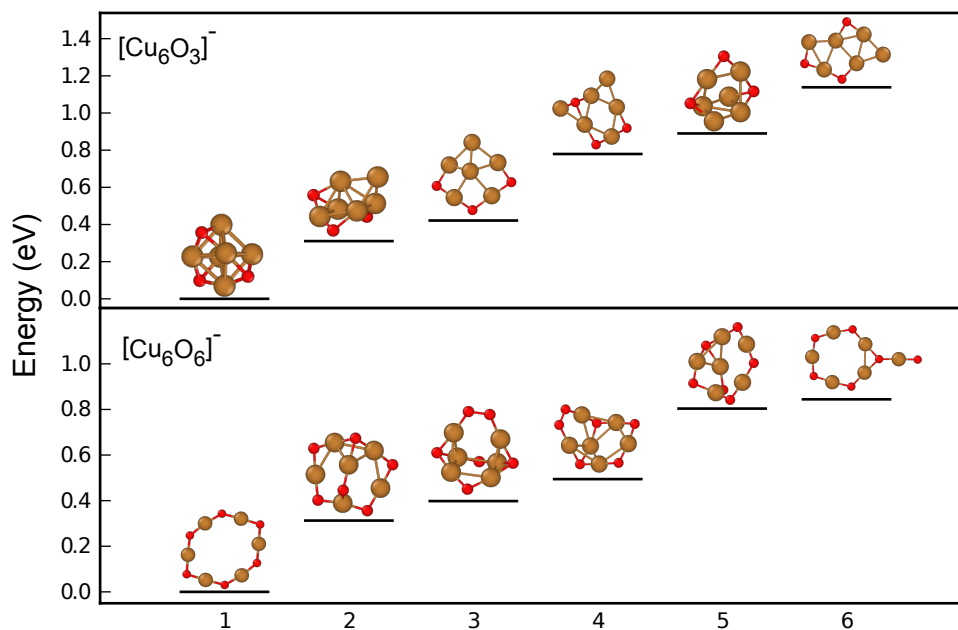


Figure A.1: Comparing top candidates after 50 GA iterations for $[\text{Cu}_6\text{O}_3]^-$ (top) and 100 GA iterations for $[\text{Cu}_6\text{O}_6]^-$ (bottom). The clusters furthest to the left are the global minima and all energies are relative to these.